# Synthesis and characterization of Pt/graphene-CNTs electrocatalyst for direct methanol fuel cell

**Richa Baronia, Shraddha Tiwari, Avanish K. Srivastava, Surinder P. Singh, Sunil K. Singhal***

*CSIR-National Physical Laboratory, Dr K.S. Krishnan Marg, New Delhi-110012, India*

*Corresponding author, E-mail: sksinghal@mail.nplindia.org; Tel: (+91) 11-45608404

**Received: 29 March 2016, Revised: 01 August 2016 and Accepted: 03 August 2016**

DOI: 10.5185/amp.2016/104
www.vbripress.com/amp

## Abstract

In the present work we report a facile method for the synthesis of Pt nanoparticles supported reduced graphene oxide (rGO) and multi-walled carbon nanotubes (MWCNTs) nanocomposite by an in-situ chemical reduction. The incorporation of MWCNTs to rGO leads to decrease in agglomeration between rGO sheets due to π – π interactions and higher loading of Pt nanoparticles. In this process, a mixture of exfoliated graphene oxide, CNTs and chloroplatinic acid was treated with a mixture of hydrazine hydrate and ammonium hydroxide at 95° C in an oil bath for 1 h. Pt nanoparticles of 4-6 nm size were homogeneously dispersed on rGO-CNTs nanocomposite as revealed by TEM analysis. Cyclic voltammetry measurements depict an anodic current density of 11.74 mA/cm$^2$ that could be obtained using Pt/rGO-CNTs catalyst and 6.2 mA/cm$^2$ using Pt/rGO catalyst during methanol oxidation, indicating that the catalytic activity of Pt/rGO-CNTs catalyst is almost 2 times higher than that of Pt/rGO catalyst. The electrochemical stability of Pt/rGO-CNTs catalyst was also found to be much higher as compared with that of Pt/rGO catalyst. Thus, Pt/rGO-CNTs catalyst has the potential to be used in the preparation of a promising anode material for direct methanol fuel cell. Copyright © 2016 VBRI Press

**Keywords** Carbon nanotubes, graphene, in-situ chemical reduction, methanol electro-oxidation, cyclic voltammetry.

## Introduction

Direct methanol fuel cells (DMFCs) have recently become attractive competitors in transportation and electrical power generation due to their high energy conversion efficiency, low operating temperature and low exhaust emission and thus are most suitable for mobile and portable electronic applications **[1-5].** In a DMFC, methanol is oxidized to carbon dioxide at the anode which is usually made of Pt or Pt supported on a carbonaceous material. Water is consumed at the anode and is produced at the cathode. Protons ($H^+$) are transported through the proton exchange membrane to the cathode where they react with oxygen to produce water. Electrons are transported from the anode to cathode, providing power to connected devices. In the development of an anode material Pt nanoparticles are normally supported on carbon black (Vulcan XC-72R), CNTs and rediced graphene oxide (rGO) because of the high specific area of Vulcan XC (~ 237 m$^2$/g, CNTs (~500-1000 m$^2$/g) and graphene (2620 m$^2$/g) **[5].** Carbon black-supported Pt was initially used as a methanol oxidation electrocatalyst for fuel cell applications, but the vulnerability toward oxidation of carbon black support hinders its use for electrode applications **[6].** Consequently, there is an increasing interest to develop new electrode material that avoids the drawbacks linked to carbon black supports. Therefore, researchers tried mainly to synthesize Pt or Pt based alloys supported on CNTs and graphene for fuel cell applications **[7-14]**. However, in all cases, synthesis of highly dispersed Pt nanoparticle on to CNTs or rGO support, still remains a challenge, especially for high metal loading. In order to synthesize Pt or Pt alloy electrocatalysts, the carbon based materials (CNTs or graphene) are first dispersed mainly in aqueous solution using ultrasonication in the presence of a Pt-salt followed by reduction using a number of reducing agents such as sodium borohydride, formaldehyde, hydrazine hydrate, ethylene glycol etc **[15-17].** It has been shown that metal (Pt) particle onto CNTs with outstanding physicochemical properties exhibited improved catalytic activity **[18].** In comparison with CNTs, graphene nanosheets not only possess similar stable properties but also large surface area, high thermal conductivity (~ 5000 W/mK) and high mobility of charge carriers (200,000 cm$^2$/Vs) **[19].** Further the production cost of rGO nanosheets is much lower than that of CNTs. Therefore, a combination of these properties along with its good dispersion stability **[20]** makes it a very attractive material for the development of Pt and/or Pt alloy

supported on rGO for the preparation of an anode material used in a DMFC. However, the rGO nanosheets in most of these methods tend to form aggregates in solution due to the π-π interaction between individual rGO sheets **[21]** making the surface area much lower in addition to lower conductivity and other mechanical properties. Therefore, the preparation of well dispersed rGO nanosheets is still a big challenge. This problem has been sorted-out in different ways, such as by the surface modification of graphene by polymer, surfactant or decoration of graphene surface with metal or metal oxides nanoparticles which reduces the π-π interaction **[22].** By incorporating CNTs between the rGO sheets π-π interaction between individual graphene sheets in greatly reduced and one can exploit the properties of graphene in a much better way.

In the present work we have incorporated CNTs to rGO nanosheets and also deposited a uniform layer of Pt nanoparticles through an in-situ chemical reduction process using a 50 vol% each of hydrazine hydrate and ammonium hydroxide as the reducing agent. The novelty of our process is that the incorporation of CNTs between rGO nanosheets not only reduced significantly the agglomeration among GO nanosheets but also enhanced the electrochemical activity of Pt/rGO-CNTs catalyst. The Pt/rGO-CNTs catalyst was characterized by various characterization techniques and its catalytic activity towards methanol electro-oxidation was evaluated by cyclic voltammetry (CV) in half-cell experiments. The performance was compared with those of graphene supported Pt catalyst prepared under similar experimental conditions.

## Experimental

*Materials*

Chloroplatinic acid hexahydrate ($H_2PtCl_6$. $6H_2O$, ammonium hydroxide solution (~ 25% $NH_3$, AR), hydrazine hydrate solution (50-60% in water, 99.99% purity), sulfuric acid (> 98%), Hydrochloric acid (35-37%), toluene (> 98%), sodium nitrate (> 98%), $KMnO_4$ (> 98%), hydrogen peroxide solution (30% in water), sodium hydroxide (> 98%), Nafion solution 117 and ferrocene (98%) were all obtained from Sigma-Aldrich. Methanol was supplied by Merck. Ultra-high purity graphite powder used for the synthesis of graphene oxide (GO) was supplied by Ultra Carbon, USA. Multi-walled carbon nanotubes (CNTs) used in this work was synthesized in our laboratory. De-ionized water was used throughout the study.

*Preparation of multi-walled carbon nanotubes and graphene oxide*

Multiwalled carbon nanotubes (CNTs) used in the present work for the synthesis of rGO/CNTs nanocomposite was synthesized in our laboratory by the thermal chemical vapor decomposition of toluene at 750°C in the presence of ferrocene catalyst **[23]**. These CNTs were functionalized by refluxing in a mixture of $HNO_3$ and $H_2SO_4$ (1:1, v/v) at about 100 °C for 4 h.

Graphene oxide (GO) was synthesized by a method as reported by a modified Hummer's method **[24, 25].** In a typical experiment 0.5 g of high purity graphite powder (Ultra Carbon, USA) was added to 23 ml $H_2SO_4$. To this solution was added 0.5 g $NaNO_3$ followed by the addition of 1.5 g of $KMnO_4$ under vigorous stirring at 0°C in order to prevent overheating and explosion. The solution was then kept at 30-40°C for 12 h under constant stirring. After that the resulting solution was diluted by adding 500 ml of deionized (DI) water. The oxidation level of graphene oxide was improved by treating the resulting mixture with 30% $H_2O_2$ (5 ml) and to remove the Mn salts. The yellow-brown mixture consisting of GO was obtained by centrifugation at 15000 rpm for 10 minutes followed by washing with dilute HCl and DI water. From a detailed experimentation it was observed that if the centrifugation was carried out at lower rpm (< 15000 rpm) the product was always contaminated with GO and unoxidized graphite (as evidenced by XRD, not shown here). GO powder was finally dried by heating it at 60°C under a vacuum oven for overnight.

*Synthesis of catalysts*

Pt/rGO-CNTs nanocomposite was prepared via the in-situ reduction of exfoliated GO and chloroplatinic acid hexahydrate in the presence of acid functionalized multiwalled CNTs using a 1:1 mixture of hydrazine hydrate and ammonium hydroxide solution **[26].** In a typical experiment a rGO-CNTs composite (2:1, w/w) was synthesized by exfoliating 200 mg of GO powder in 100 ml DI water by ultrasonication for 1 h followed by the addition of 100 mg of acid functionalized CNTs and the mixture was stirred for another 1 h. In another beaker 60 mg of chloroplatinic acid hexahydrate was dissolved in 10 ml of DI water and neutralized by adding 1M NaOH in order to achieve a pH of 11.7. This solution was then added very slowly to the flask containing exfoliated GO and CNTs. The resulting mixture was reduced by the addition of 1:1 mixture of hydrazine hydrate and ammonium hydroxide (10 ml each) and then heated at 95 °C for 1 h in an oil bath. After the completion of reaction, the product consisting of Pt nanoparticles deposited on rGO/CNTs hybrid was obtained by filtration and dialysis. The filtration was carried out under vacuum through a polyvinylidene fluoride membrane filter (25 nm in diameter, 0.45 µm pore size; Millipore). Similar procedure was used for the synthesis of Pt nanoparticles upported on rGO. Different steps involved in synthesis of Pt/rGO/CNTs are shown in **Schematic. 1**.

*Physicochemical characterization*

 

The crystal structure identification of various samples synthesized in the present work was determined using powder X-ray diffraction (XRD) on a Rigaku Miniflex 600 diffractometer using CuKα radiation (λ = 0.15405 nm) under a voltage of 40 kV and a current of 30 mA. The diffraction data was recorded for 2θ angle between 5 and 80° with a scan rate of 2°/min to ensure obtaining fine crystalline structure of graphene oxide (GO), rGO and Pt nanoparticles. In order to estimate the particle size of Pt nanoparticles from XRD, using the Scherrer's formula. Surface morphology of Pt nanoparticles and their dispersion on rGO/CNTs hybrid material was studied using a scanning electron microscope (SEM, Model No. VP-EVO, MA-10, Carl-Zeiss, UK) equipped with energy dispersive spectrometer and microstructural properties using a high resolution transmission electron microscope (TEM) (Model No. FEI, Tecnai T30) operated at an accelerating voltage of 300 kV. The samples for TEM characterization were prepared by dispersing Pt/rGO-CNTs electrocatalyst in ethanol using ultrasonication for about 10 min followed by drop casting a small amount on a 400-mesh carbon-coated copper grid and letting it dry in air.

The GO and Pt/rGO-CNT electrocatalyst synthesized in the present work were also characterized using Raman spectroscopy (Model: using a Renishaw inVia Reflex Raman spectrometer, UK) with an excitation laser source of 514 nm wavelength. The Raman spectra were recorded from 1000 $cm^{-1}$ to 3000 $cm^{-1}$ with 5 mW laser power and 10s of exposure time. The analysis of various functional groups attached on to the surface of GO was studied by Fourier transform infrared spectroscopy (FTIR) (Model: Cary 630, Agilent Technologies, USA) by recording the spectra from 500 $cm^{-1}$ to 4000 $cm^{-1}$. The exact loading of Pt in the synthesized catalysts was determined by atomic mass spectrometer (Model: AAS, Vario 6, Analytik Jena, Germany).

The electrochemical activity of Pt nanoparticles supported on rGO and rGO/CNTs hybrid were measured in a conventional three-electrode cell using a PalmSens, electrochemical work station. The three-electrode cell was composed of a glassy carbon (GC) disk (3 mm diameter, surface area 0.070 $cm^2$) coated with the catalyst as the working electrode, Ag/AgCl as a reference electrode and a platinum mesh was as a counter electrode. The working electrode was prepared by dispersing 2.5 mg of the catalyst powder in the mixed solution (300 µL ethanol and 200 µL Nafion 117 solution) using ultrasonication for 1 h to form a homogeneous ink, and 5 µL of the resulting electrocatalyst ink was carefully dropped onto the GC electrode surface, then the coating was dried in air at room temperature.

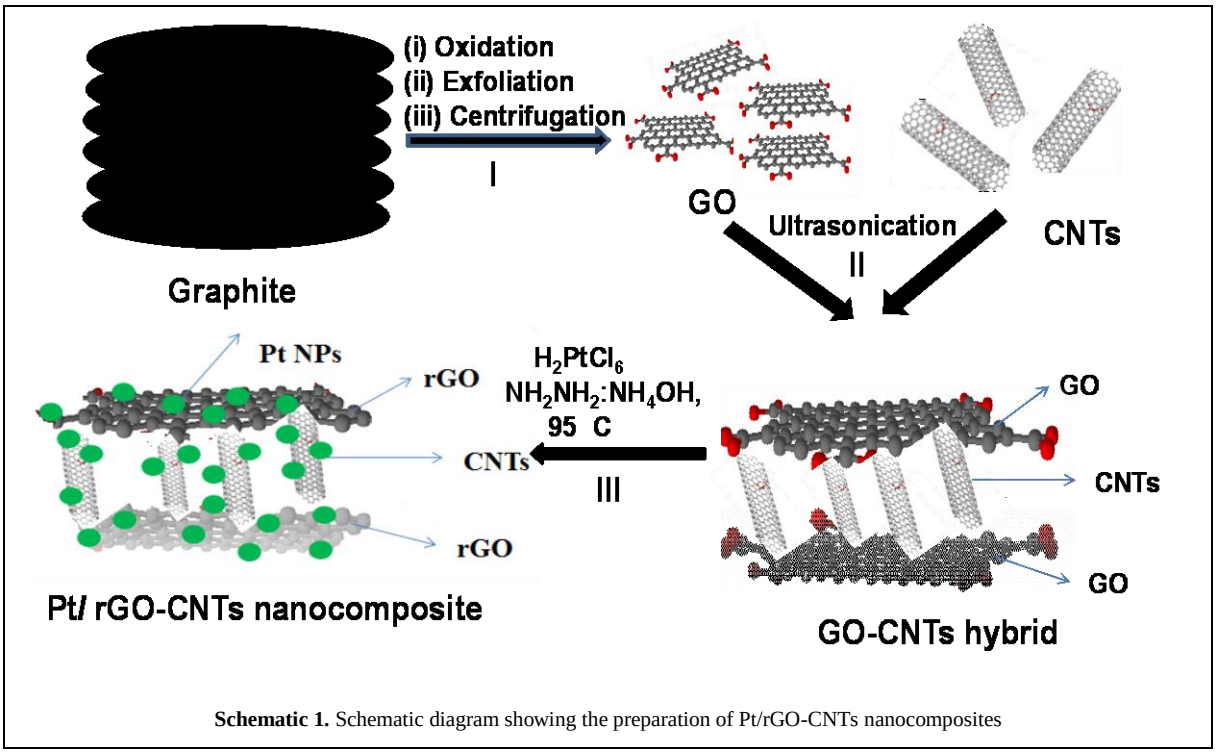


**Schematic 1.** Schematic diagram showing the preparation of Pt/rGO-CNTs nanocomposites

The electrochemical surface area (ECSA) of Pt in Pt/rGO and Pt/rGO-CNTs catalysts were assessed by cyclic voltammograms of the hydrogen adsorption in a $N_2$ saturated 1M $H_2SO_4$ solution and the electrochemical activity for methanol oxidation reaction was measured in a solution containing 2M $CH_3OH$ and 1M $H_2SO_4$ at a scan rate of 70 mV/s between -0.2 V to 1.0 V. All the measurements were carried out at room temperature.

## Results and discussion

*Physicochemical characterization: Graphene oxide and reduced graphene oxide*

**Fig. 1** shows the XRD patterns of precursor graphite, GO powder, reduced graphene oxide (rGO) and rGO-CNTs hybrid nanocomposite. Graphite exhibited a characteristic (002) diffraction peak at 26.6°, **Fig.**

 

**1(a),** corresponding to a interspacing between the two layers as 0.337 nm (JCPDS: 14-1487). Upon oxidation/exfoliation of graphite with strong acids, the ordering of the graphene layers in graphite was disrupted and a smaller broader peak appeared at 2θ = 11.24 ° (characteristic of GO) as shown in **Fig. 1b**. The interlayer spacing between the layers in GO is increased from 0.337 nm to 0.789 nm. This is mainly due to the incorporation of various functional groups and water molecules bonded on both sides of graphene oxide sheets. The disappearance of graphitic peak also ensures the complete oxidation of graphite into GO. After chemical reduction with a mixture of hydrazine hydrate and ammonium hydroxide, GO was reduced to graphene or reduced graphene oxide (rGO) with a characteristic peak at 2θ = 24.86° (d-spacing: 0.341 nm) as shown in **Fig. 1c**. The interlayer spacing in rGO was still little higher than the d-spacing of graphite (0.337 nm). This is mainly because of the presence of small amount of functional groups and the remaining of hydrogen, indicating incomplete reduction of GO into rGO. **Fig. 1d** shows a typical XRD pattern of rGO-CNTs nanocomposite synthesized in the present work. In this XRD pattern the diffraction peak of rGO-CNTs composite appeared at 2 θ = 25.1° (d-spacing: 0.3546 nm). It can be seen that the interlayer spacing observed in rGO-CNTs composite is still higher as compared with those observed for rGO (0. 341 nm) and graphite (0.337 nm).

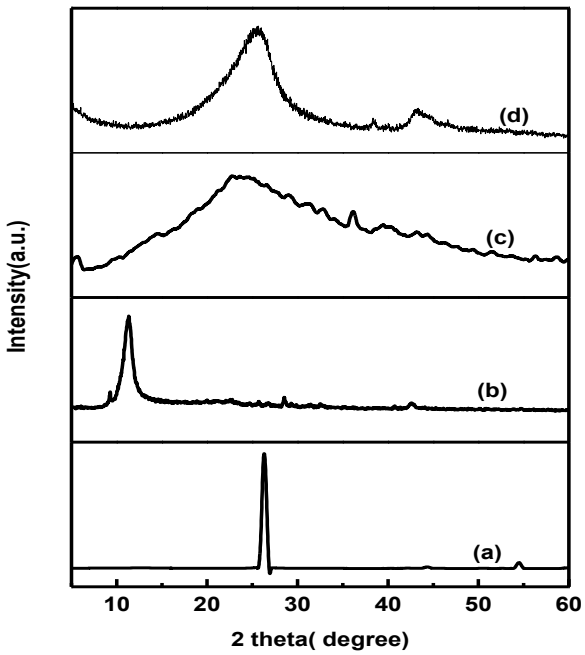


**Fig. 1.** XRD patterns of (a) graphite, (b) graphene oxide, (c) reduced graphene oxide (rGO), and (d) rGO-CNTs composite.

Further, various functional groups attached onto the surface of GO and rGO were studied using FTIR. **Fig. 2a** shows a typical FTIR spectra of GO and rGO synthesized in the present work. The absorption bands observed at 3245, 1720, 1624, 1375, 1229 and 1043 $cm^{-1}$ are associated with O-H stretching, C=O stretching, aromatic C=C bending, C-O stretching, C-O-C stretching, C-OH stretching vibrations in GO respectively. After the reduction with a mixture of hydrazine hydrate and ammonium hydroxide the intensity of absorption bands due to various functional groups present in GO decreased significantly and the absorption band corresponding to C=C vibration shifted from 1620 $cm^{-1}$ to 1600 $cm^{-1}$ [**27**].

**Fig. 2(b)** represents the UV visible spectra of GO and rGO synthesize in the present work. In UV visible spectra of GO two characteristic peaks are attributed to $\pi$-$\pi^*$ transitions of C=C bond at 230 nm and n-$\pi^*$ transitions of C=O at 300 nm. In case of rGO the peak observed at 230 nm ($\pi$-$\pi^*$ transitions of C=C bond) shifted to 270 nm because of the reduction of GO and restoration of the conjugated aromatic system.

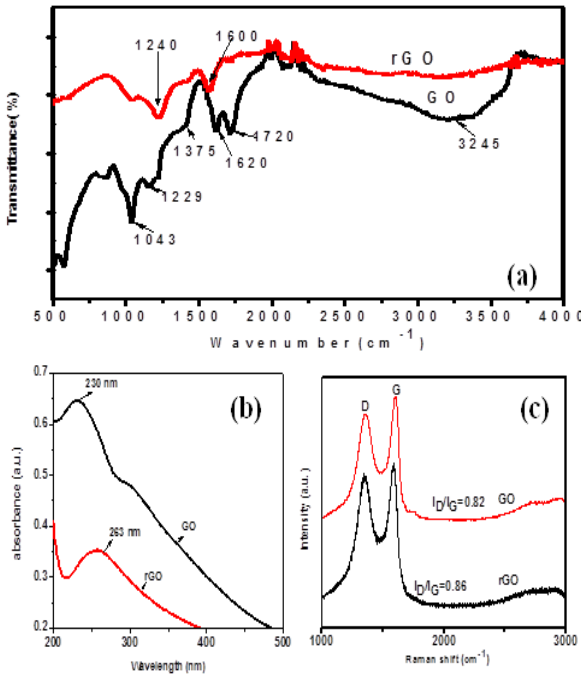


**Fig. 2** FTIR (a), UV-vis (b) and Raman spectra (c) of GO and rGO

GO and rGO were also characterized by using Raman spectroscopy. It is a very useful technique to characterize various carbonaceous materials, specially distinguishing between graphene and graphite **[29].** The D- band and G -band in the Raman spectra are attributed to $sp^2$ and $sp^3$ carbon stretching modes and their intensity ratio ($I_d/I_g$) is a measure of the amount of disorder present in the material. For pure graphite the G -band and D- band are observed at 1580 and 1350 $cm^{-1}$ in the Raman spectrum (not shown here). **Fig. 2(c)** shows a typical Raman spectrum of GO and rGO synthesized in the present work. In case of GO, G- band was up shifted to 1592 $cm^{-1}$ compared with that of graphite 1580 $cm^{-1}$. However, after the reduction of GO, the G -band in rGO appeared at 1586 $cm^{-1}$, due to the recovery of hexagon network of carbon atoms with defects. After the reduction of GO into rGO, the intensity ratio of G and D- band ($I_d/I_g$) of graphene was increased from

 

0.82 to 0.86 indicating the reduction process altered the structure of GO. This phenomenon could be attributed to significant decrease of size of the in-plane $sp^2$ domains due to oxidation and ultrasonic exfoliations and partially ordered graphite crystal structure of graphene sheets **[29].**

*Characterization of Pt/rGO-CNTs electrocatalyst*

**Fig. 3(a)** shows typical XRD pattern for Pt/rGO-CNTs nanocomposites synthesized in the present work. The diffraction peak at 2θ= 25.57° corresponds to the (002) plane of graphitized carbon. After chemical reduction using a mixture of hydrazine hydrate and ammonium hydroxide, the diffraction pattern observed for GO (2θ= 11.24°) was disappeared and a broader (002) diffraction peak at 2θ =25.57° was observed. It clearly indicates the removal of oxygen-containing functional groups and water molecules and formation of randomly ordered graphene. Also, the broadening of (002) diffraction peak indicates the smaller size of graphene compared to the original graphite powder and GO. The other diffraction peaks observed at 2θ values of 39.68, 46.24 and 81.28° can be attributed to (111), (200) and (311) planes, respectively are attributed to face-centered-cubic crystallographic structure of Pt [JCPDS 4-802]. From this figure it is seen that there is a small change in the position of (002) diffraction plane for rGO/CNTs hybrid than those observed for graphene. The slight shift in 2θ values observed for rGO/CNTs hybrid in the XRD pattern indicates the formation of a strong interaction between rGO and CNTs.

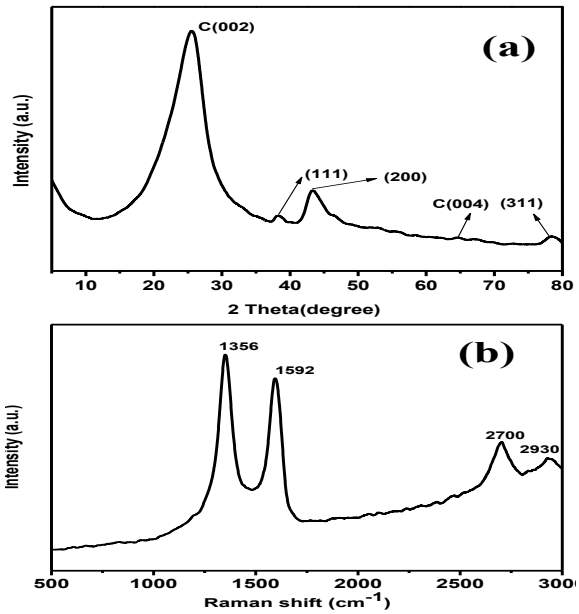


**Fig.3**. (a) XRD pattern (b) Raman spectra of Pt/rGO-CNTs

The incorporation of CNTs causes the development of some stresses in the rGO nanosheets and causes a shift in 2θ value. These results were further confirmed by measuring the shift of D and G bands in the Raman spectrum and TEM characterization of Pt/rGO-CNTs electrocatalyst. The diffraction peak for Pt (200) was used to estimate the average Pt particle size using the Scherrer's equation: $D = \frac{0.89\lambda}{\beta\cos\theta}$, Here the wavelength λ is equal to 0.15418 nm and β is the full width at half-maximum (FWHM). The calculated average particle size of Pt nanoparticles on graphene/CNTs hybrid composite was found to be ~ 5 nm.

**Fig. 3(b)** shows a typical Raman spectrum of Pt/rGO-CNTs electrocatalyst. The G-band observed at 1592 $cm^{-1}$ was mainly due to $sp^2$ hybridized carbon atoms and D-band at 1356 $cm^{-1}$ was due to the defects present. The G-band of pure graphite is mainly observed at 1580 $cm^{-1}$, so the shifting in the frequency of 12 $cm^{-1}$ in the rightward direction may be due to the reduction in size of the in-plane $sp^2$ domains possibly due to strong oxidation. It is also likely that the presence of isolated double bonds in rGO/CNT hybrid resonate at frequencies higher than that of the G-band of graphite **[29]**. The $I_d/I_g$ ratio for GO is 1.09 whereas the $I_d/I_g$ ratio rGO-CNTs hybrid composite is increased to 1.166 **Fig. 3(b)** and is due to more defects introduced. The shift and shape of the overtone of the D-band, called the 2D band around 2700 $cm^{-1}$ can be correlated to the number of GO layers. Weak and broad 2D peak is the indication of disorder. A defect activated peak, called the (D+G) band is also observed near 2930 $cm^{-1}$ in the Raman spectrum.

*SEM & TEM characterization of Pt/rGO-CNTs nanocomposites*

**Fig. 4 (a)** and **(b)** shows a typical SEM micrograph of GO and Pt/rGO-CNTs nanocomposites synthesized in the present work. In the SEM micrograph shown in **Fig. 4a** the GO nanosheets form randomly aggregated thin sheets. **Fig. 4b** shows a typical SEM image of Pt/rGO-CNTs composite in which the grphene nanosheets of wrinkled morphology forms a homogeneous network between CNTs. Pt nanoparticles are seen uniformly distributed on rGO/CNTs hybrid. These CNTs prevent the aggregation of rGO nanosheets due to van der Waals forces and maintain high surface area **[30, 31]**. The CNTs not only prevent the aggregation of GO nanosheets but also increases the distance between graphene layers. **Fig. 4c** shows a typical TEM image of Pt/rGO-CNTs composite. Pt nanoparticles are deposited on CNT/rGO hybrid with almost uniform dispersion. In the HR-TEM image shown in **Fig.4d** it is seen that most voids within CNTs network are covered with rGO nanosheets. The d-spacing value of 0.23 nm concides with that of fcc Pt (111). The average size of Pt nanoparticles estimated from TEM images are ~ 5 nm on CNT/rGO hybrid and is in agreement with XRD results.

All electrochemical measurements were performed using cyclic voltammetry (CV) at room temperature. The electrochemically active surface area (ECSA) of an electrocatalyst provides important information regarding the number of available electrochemically

 

active sites that are necessary for evaluating the electrocatalytic activity. The ECSA values for Pt/rGO and Pt/rGO-CNTs catalysts recorded using CV in a 1M sulfuric acid with scan rate of 70 mV/s between 0.2 V and 1.2 V vs Ag/AgCl.

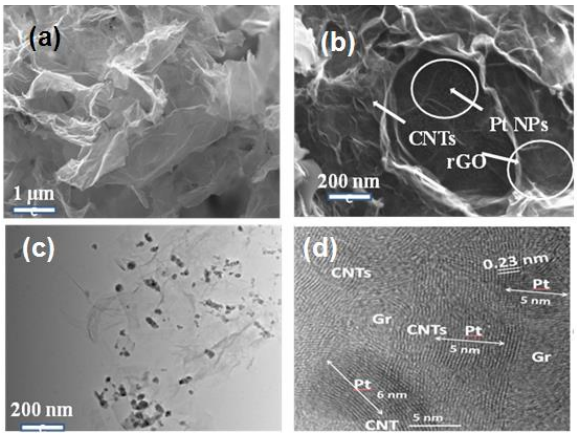


**Fig 4** SEM images of (a) rGO (b) Pt-rGO/CNT catalyst (c) TEM (d) HR TEM images Pt-rGO/CNT catalyst

The integrated area under the adsorption peak in the CV curves represent the total charge associated with $H^+$ adsorption on Pt and the ECSA was evaluated using the following equation **[32]:**

ECSA ($cm^2$/g of Pt) = Charge [$Q_H$, µC/$cm^2$] / 210 (µC/$cm^2$) x electrode loading (g of Pt/$cm^2$)

where $Q_H$ is the charge for hydrogen adsorption and 210 represents the charge required a monolayer of $H_2$ on bright Pt (µC/$cm^2$). The Pt loading in Pt/rGO and Pt/rGO-CNTs catalysts was determined by AAS and found to be 0.00031 g/$cm^2$.

**Fig. 5a** shows the CV curves for GO, Pt/rGO-CNTs and Pt/rGO catalysts in 1M $H_2SO_4$ at a scan rate 70 mV/s. using this equation, the ECSA for Pt/rGO-CNTs (65.89 $m^2$/g) was found to be much higher than that of Pt/rGO catalyst (31.79 $m^2$/g), clearly demonstrating that Pt/rGO-CNTs possesses much higher electrochemical activity than Pt/rGO catalyst.

*Methanol electro-oxidation*

The catalytic activities of GO, Pt/rGO-CNTs and Pt/rGO catalysts towards methanol oxidation were evaluated using CV in a solution containing 2M $CH_3OH$ and 1M $H_2SO_4$ with a scan rate of 70 mV/s between – 0.2 V to 1.0 V vs Ag/AgCl at room temperature. The CV curves for both electro catalysts for methanol electro-oxidation are shown in **Fig. 5b**. The CV curves for both the catalysts show similar methanol electro-oxidation anodic current peak in the forward scan ($I_f$) and an oxidation peak in the backward scan ($I_b$) corresponding to the removal of residual carbonaceous intermediates formed in the forward scan. It can be seen that the forward current density (11.74 mA/$cm^2$) of Pt/rGO-CNTs catalyst is much higher than that of Pt/rGO catalyst (6.2 mA/$cm^2$). Further, the oxidation potential of methanol oxidation observed for Pt/rGO/CNTs catalyst was lower (0.65 V) as compared with that observed for Pt/rGO catalyst (0.68 V). This observation again suggests that the incorporation of CNTs in rGO decreases the barrier to methanol oxidation, and thus, Pt/rGO-CNTs catalysts performs better than Pt/rGO catalyst and is in consistent with the ECSA results. A very small current density was observed for pure GO electrode.

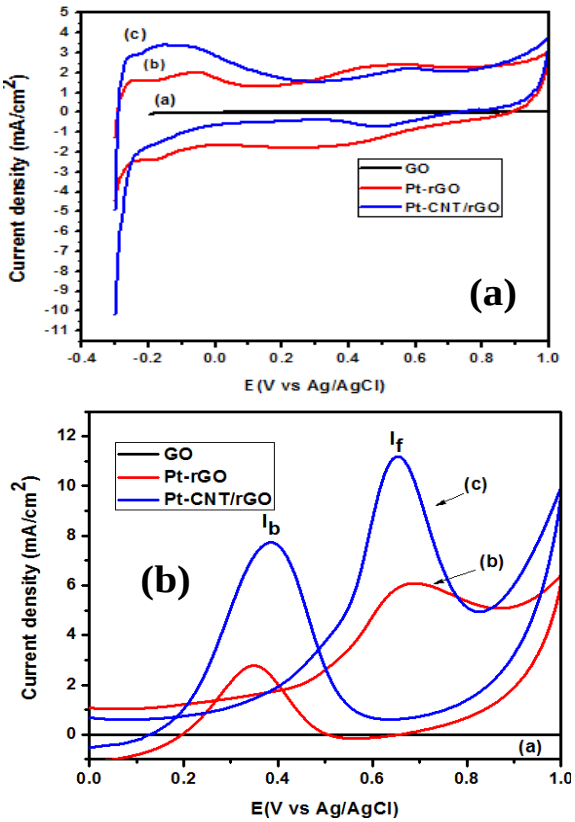


**Fig.5**.Cyclic voltamograms in **(a)** 1M $H_2SO_4$ solution at a scan rate of 70 mV/s (a) GO (b) Pt-/rGO and (c) Pt/rGO-CNT catalysts and **(b)** methanol electro-oxidation curves in 1M $H_2SO_4$ and 2M $CH_3OH$ solution at a scan rate of 70 mV/s (a) GCE (b) Pt-rGO and (c) Pt/rGO-CNT catalysts

On the basis of above experimental results it is demonstrated that Pt/rGO-CNTs has better electrochemical activity and long term stability than commercially available Pt/rGO catalyst presumably due to i) larger ECSA values of Pt/rGO-CNTs ii) high dispersion of Pt nanoparticles and iii) low agglomeration of graphene nanosheets in rGO/CNTs hybrid by the incorporation of CNTs between graphene layers.

## Conclusion

In summary, we have demonstrated a facile synthesis of a Pt/rGO-CNTs electrocatalyst by a simultaneous chemical reduction process using a mixture of hydrazine hydrate and ammonium hydroxide as the reducing agents. Using this method, the CNTs are incorporated between the GO nanosheets, thereby preventing their aggregation. The three dimensional graphene-CNTs nanocomposite comprises a network with ultrathin GO sheets between the CNTs bundles

 

as revealed by SEM characterization. This electrocatalyst was found to possess much better electrochemical activity, larger ECSA values than those observed for Pt/rGO catalyst presumably because of non-agglomeration of rGO nanosheets in rGO-CNTs nanocomposite. The results show that Pt/rGO-CNTs catalyst could be used as a promising anode material for a direct methanol fuel cell and may find applications in the fabrication of many devices such as sensors, batteries and super capacitors.

**Acknowledgements**

This research work was supported by Council of Scientific and Industrial Research (CSIR), New Delhi, India under the CSIR-Emeritus Scientist Scheme. The authors are grateful to the Director, CSIR-NPL to provide different facilities to carry out this work. Sincere thanks are due to Dr. Nahar Singh, Mr. Naval Kishore Upadhyaya, Mr. K. N. Sood, Ms Shweta Sharma and Dr. Priti Singh for their help in atomic absorption spectroscopy analysis of Pt in Pt/rGO and Pt/rGO-CNTs electrocatalysts, XRD, SEM, Raman spectroscopy and cyclic voltammetry measurements of various samples prepared in the present work. SPS acknowledge the funding from NanoSHE, BSC0112.

**References**

1. Chen, I.; Minett A.I.; Liu, Y.; Lynam, C., Sherrel, P.; Wang, C.Y.; Wallace, G.G.; *Adv. Mater*., **2008,** *20, 566.* **DOI:** 10.1002/adma.200701146
2. Noel, M.; Suryanarayanan, V.; *J. Power Sources*, **2002,** *111, 193.* **DOI:** 10/1016/s0378-7753(02)00308-7
3. Zhang, J.; Liu, H.; (Eds), Electrolysis of Direct Methanol Fuel Cells: From Fundamentals to Applications, Wiley, USA, Sept. **2009.**
4. Arico, A.S.; Baglio, V.; Antonucci, V.; Direct Methanol Fuel Cells (Energy, Science, Engineering and Technology), Nova Science Publishers, Inc., USA, April, **2010.**
5. Li, Y.; Tang, L.; Li, J.; *Electr. Commun.* **2009,** *11, 846.* **DOI:** 10.1016/j.elecom.2009.02.009
6. Maass, S.; Finsterwalder, F.; Frank, G.; Hartmann, R.; Merten, C.; *J Power Sources*, **2008,** 176, 444. **DOI:** 10.1016/j/jpowsour.2007.08.053
7. Qian, W.; Hao, R.; Zhou, J.; Eastman, M.; Manhat, B.A.; Sun, Q.; Goforth, A.M.; Jiao, J.; *Carbon*, **2013,** 52, 595. **DOI:** 10.1016/j.carbon, 2012.10.031
8. Gao, H.; He, L.; Xiao, Y.; Zhang, Y.; Zhang, S.; *Ionics*, **2016,** 1. **DIO:** 10.1007/s11581-016-1727-9
9. Dong, L.; Gari, R.R.S.; Li, Z.; Craig, M.M.; Hou, S.; *Carbon*, **2010,** 48, 781. **DOI:** 10.1016/j.carbon.2009.10.027
10. Li, Y.; Gao, W.; Ci, L.; Wang, C.; Ajayan, P.M.; *Carbon*, **2010,** 48, 1124. **DIO:** 10.1016/j.carbon.2009.11.034
11. HuaXie, H.; DongPing, S.; Xin, W.; *Chinese Science Bulletin*, **2012,** 57, 3071. **DOI:** 10.1007/s11434-012-5327-4
12. Wang, H.; Liang, Zhu, L.; Peng, F.; Yu, H.; Yang, J.; *Fuel Cells*, **2010,** 10, 99. **DOI:** 10.1002/fuce.200900112
13. Hamnett, A.; Direct methanol fuel cells, DMFC), in: Handbook of Fuel Cells Wiley, USA, **2010.** **DOI:** 10.1002/9780470974001.f104017
14. Hofstead-Duffy, A.M.; Chen, D.J.; Sun, S.G.; Tong, Y.Y.J; *J Mater Chem* **2012,** 22, 5205. **DOI:** 10.1039/c2jm15426a
15. Kim, P.; Joo, J.B.; Kim, W.; Kim, J.; Song, I.K.; Yi, J.; *J. Power Sources*, **2006,** 160, *987.* **DOI:** 10.1016/j.power.2006.02.050
16. Rao, C. V.; Reddy, A. L. M.; Ishikawa,Y.; Ajayan, P. M.; *Carbon*, **2011,** *4 9, 9 3 1.* **DOI:** 10-1016/j.carbon.2010.10.056
17. Moon, I. K.; Lee, J.; Ruoff, R.S.; Lee, *Nature Commun.*, **2010,** 73, 1. **DOI:** 10.1038/ncomms1067
18. Han, K.I.; Lee, J.S.; Park, S.O.; Lee, S.W.; Park, Y.W.; Kim, H.S.; *Electrochim. Acta*, **2004,** *50, 791.* **DOI:** 10.1016/j.electacta.2005.04.042
19. Park, S.; Ruoff, R.S.; *Nat. Nanotechnol.* **2009,** *4, 217.* **DOI:** 10.1038/nnano.2009.58
20. Stankovich, S.; Dikin, D.A.; Dmmett, G.H.B.; Kohlhaas, K.M.; Zimmey, E.J.; Stach, E.A.; Piner, R.D.; Nguyen, S.T.; Ruoff, R.S.; *Nature*, **2006,** *442, 282.* **DOI:** 10.1038/nature04969
21. Li, D.; Muller, M.B.; Gilje, S.; Kaner, R.B.; Wallace, G.G.; *Nat. Nanotechnol.*, **2008,** *3, 101.* **DOI:** 10.1038/nnano.2007.451
22. Fang, M.; Wang, K.; Lu, H.; Yang, Y.; Nutt, S.; *J. Mater. Chem*., **1982,** *20, 1982.* **DOI:** 10.1039/B919078C
23. Mathur, R.B.; Chatterjee, S.; Singh, B.P.; *Comp Sci Technol*, **2008,** 68, 1608. **DOI:** 10.1016/j.compscitech.2008.02.020
24. Hummers, W.S.; Offeman, R.E.; *J. Am. Chem. Soc.*,**1958,** *80, 1339.* **DOI:** 10.1021/ja01539a017
25. Karthikeyan, K.; Mohan, R.; Kim, S.J.; *Appl. Phys. Lett.*, **2011,** *98, 244101.* **DOI:** 10.1063/1.3599453
26. Woo, S.; Kim, Y.R.; Chung, T.D.; Piao, Y.; Kim, H.; *Electrochim. Acta.*, **2012,** *59, 509.* **DOI:** 10.1016/j/electacta.2011.11.012
27. Maillard, F,; Lu, G.Q.; Wieckowski, A.; Stimming, U.; *J. Phys. B*, **2005,** 109, 16243. **DOI:** 10.1021/jp052277x
28. Zhang, L.; Li, X.; Huang, Y.; Ma, Y.; Wan, X.; Chen, Y.; *Carbon*, **2010,** *48, 2367.* **DOI:** 10.1016/j.carbon.2010.02.035
29. Ferrari, A.C.; Robertson, J.; *Phys. Rev. B*, **2000,** *61, 14095.* **DOI:** 10.1103/PhysRevB.61.14095
30. Schniepp, H.C.; Li, J. L.; McAllister, M.J.; Sai, H.; Herrera-Alonso, M.; Adamson, D.H.; Prud'homme, R.K.; Car, R.; Saville, D.A.; Aksay, I.A.; *J. Phys. Chem. B*, **2006,** *110, 8535.* **DOI:** 10.1021/jp060936f
31. McAllister, M.J.; Li, J. L.; Adamson, D.H.; Schniepp, H.C.; Abdala, A.A.; Liu, J.; Herrera-Alonso, M.; Milius, D.L.; Car, R.; Prud'homme, .R.K.; Aksay, I.A.; *Chem. Mater.***2007,** *19, 4396.* **DOI:** 10.1021/cm0630800
32. Lee, E.P.; Peng, Z.M.; Cate, D.M.; Yang, H.; Campbell, C.T.; Xia, Y.N.; *J. Am. Chem. Soc.*, **2007,** *129, 10634.* **DOI:** 10.1021/ja074312e